Anna Esposito · Marcos Faundez-Zanuy ·
Francesco Carlo Morabito · Eros Pasero
Editors

Neural Approaches to Dynamics of Signal Exchanges

Springer

Editors
Anna Esposito
Department of Psychology
University of Campania Luigi Vanvitelli
Caserta, Italy

International Institute for Advanced
Scientific Studies (IIASS)
Italy

Francesco Carlo Morabito
Department of Civil, Environment, Energy
and Materials Engineering
Mediterranea University of Reggio Calabria
Reggio Calabria, Italy

Marcos Faundez-Zanuy
Tecnocampus
Mataró, Spain

Eros Pasero
Dipartimento di Elettronica e
Telecomunicazioni
Politecnico di Torino
Turin, Italy

ISSN 2190-3018 ISSN 2190-3026 (electronic)
Smart Innovation, Systems and Technologies
ISBN 978-981-13-8949-8 ISBN 978-981-13-8950-4 (eBook)
https://doi.org/10.1007/978-981-13-8950-4

This Springer imprint is published by the registered company Springer Nature Singapore Pte Ltd.
The registered company address is: 152 Beach Road, #21-01/04 Gateway East, Singapore 189721, Singapore

Chapter 27
Infinite Brain MR Images: PGGAN-Based Data Augmentation for Tumor Detection

Changhee Han, Leonardo Rundo, Ryosuke Araki, Yujiro Furukawa, Giancarlo Mauri, Hideki Nakayama and Hideaki Hayashi

Abstract Due to the lack of available annotated medical images, accurate computer-assisted diagnosis requires intensive data augmentation (DA) techniques, such as geometric/intensity transformations of original images; however, those transformed images intrinsically have a similar distribution to the original ones, leading to limited performance improvement. To fill the data lack in the real image distribution, we synthesize brain contrast-enhanced magnetic resonance (MR) images—realistic but completely different from the original ones—using generative adversarial networks (GANs). This study exploits progressive growing of GANs (PGGANs), a multistage generative training method, to generate original-sized 256×256 MR images for convolutional neural network-based brain tumor detection, which is challenging *via* conventional GANs; difficulties arise due to unstable GAN training with high resolution and a variety of tumors in size, location, shape, and contrast. Our preliminary results show that this novel PGGAN-based DA method can achieve a promising performance improvement, when combined with classical DA, in tumor detection and also in other medical imaging tasks.

C. Han (✉) · H. Nakayama
Graduate School of Information Science and Technology,
The University of Tokyo, Tokyo, Japan
e-mail: han@nlab.ci.i.u-tokyo.ac.jp

L. Rundo · G. Mauri
Department of Informatics, Systems and Communication,
University of Milano-Bicocca, Milan, Italy

L. Rundo
Institute of Molecular Bioimaging and Physiology (IBFM),
Italian National Research Council (CNR), Cefalù (PA), Italy

R. Araki
Graduate School of Engineering, Chubu University, Aichi, Japan

Y. Furukawa
Kanto Rosai Hospital, Kanagawa, Japan

H. Hayashi
Department of Advanced Information Technology, Kyushu University, Fukuoka, Japan

A. Esposito et al. (eds.), *Neural Approaches to Dynamics of Signal Exchanges*,
Smart Innovation, Systems and Technologies 151,
https://doi.org/10.1007/978-981-13-8950-4_27

27.1 Introduction

Along with classical methods [1, 2], convolutional neural networks (CNNs) have dramatically improved medical image analysis [3, 4], such as brain magnetic resonance imaging (MRI) segmentation [5, 6], primarily thanks to large-scale annotated training data. Unfortunately, obtaining such massive medical data is challenging; consequently, better training requires intensive data augmentation (DA) techniques, such as geometric/intensity transformations of original images [7, 8]. However, those transformed images intrinsically have a similar distribution with respect to the original ones, leading to limited performance improvement; thus, generating realistic (i.e., similar to the real image distribution) but completely new samples is essential to fill the real image distribution uncovered by the original dataset. In this context, generative adversarial network (GAN)-based DA is promising, as it has shown excellent performance in computer vision, revealing good generalization ability. Especially, SimGAN outperformed the state of the art with 21% improvement in eye gaze estimation [9].

Also in medical imaging, realistic retinal image and computed tomography (CT) image generation have been tackled using adversarial learning [10, 11]; a very recent study reported performance improvement with synthetic training data in CNN-based liver lesion classification, using a small number of 64×64 CT images for GAN training [12]. However, GAN-based image generation using MRI, the most effective modality for soft-tissue acquisition, has not yet been reported due to the difficulties from low-contrast MR images, strong anatomical consistency, and intra-sequence variability; in our previous work [13], we generated $64 \times 64/128 \times 128$ MR images using conventional GANs and even an expert physician failed to accurately distinguish between the real/synthetic images.

So, how can we generate highly realistic and original-sized 256×256 images, while maintaining clear tumor/non-tumor features using GANs? Our aim is to generate GAN-based synthetic contrast-enhanced T1-weighted (T1c) brain MR images—the most commonly used sequence in tumor detection thanks to its high contrast [14, 15]—for CNN-based tumor detection. This computer-assisted brain tumor MRI analysis task is clinically valuable for better diagnosis, prognosis, and treatment [5, 6]. Generating 256×256 images is extremely challenging: (*i*) GAN training is unstable with high-resolution inputs, and severe artifacts appear due to strong consistency in brain anatomy; (*ii*) brain tumors vary in size, location, shape, and contrast. However, it is beneficial, because most CNN architectures adopt around 256×256 input sizes (e.g., Inception-ResNet-V2 [16]: 299×299, ResNet-50 [17]: 224×224) and we can achieve better results with original-sized image augmentation—toward this, we use progressive growing of GANs (PGGANs), a multistage generative training method [18]. Moreover, an expert physician evaluates the generated images' realism and tumor/non-tumor features *via* the visual Turing test [19]. Using the synthetic images, our novel PGGAN-based DA approach achieves better performance in CNN-based tumor detection, when combined with classical DA (Fig. 27.1).

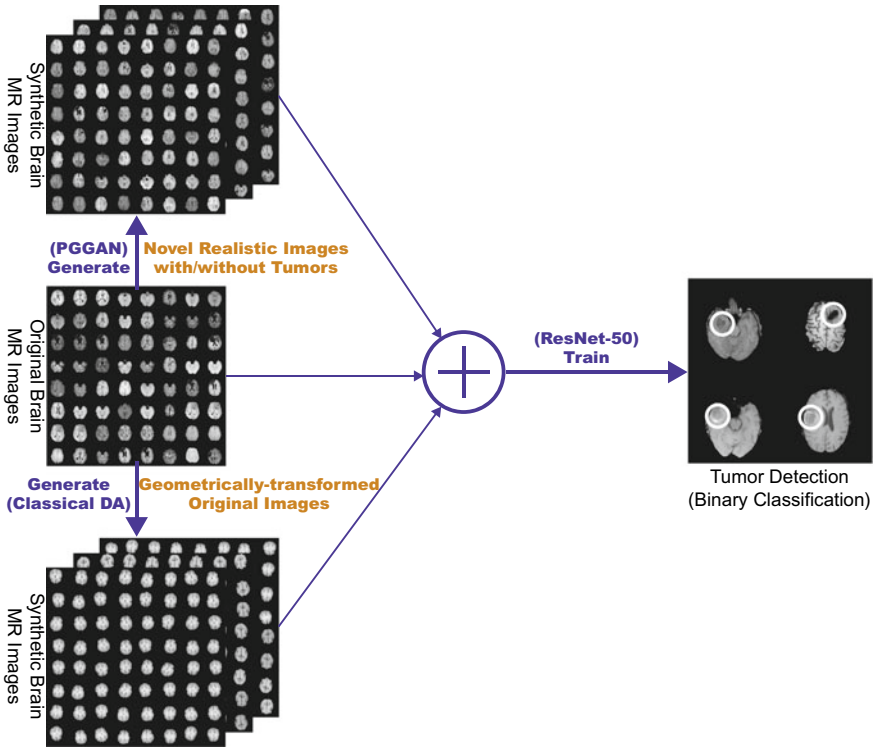

Fig. 27.1 PGGAN-based DA for better tumor detection: The PGGANs method generates a number of realistic brain tumor/non-tumor MR images, and the binary classifier uses them as additional training data

Contributions. Our main contributions are as follows:

- **MR Image Generation**: This research explains how to exploit MRI data to generate realistic and original-sized 256×256 whole-brain MR images using PGGANs, while maintaining clear tumor/non-tumor features.
- **MR Image Augmentation**: This study shows encouraging results on PGGAN-based DA, when combined with classical DA, for better tumor detection and other medical imaging tasks.

The rest of the manuscript is organized as follows: Sect. 27.2 introduces background on GANs; Sect. 27.3 describes our MRI dataset and PGGAN-based DA approach for tumor detection with its validations; experimental results are shown and analyzed in Sect. 27.4; Sect. 27.5 presents conclusion and future work.

27.2 Generative Adversarial Networks

Originally proposed by Goodfellow et al. in 2014 [20], GANs have shown remarkable results in image generation [21] relying on a two-player minimax game: A generator network aims at generating realistic images to fool a discriminator network that aims at distinguishing between the real/synthetic images. However, the two-player objective function leads to difficult training accompanying artificiality and mode collapse [22], especially with high resolution. Deep convolutional GAN (DCGAN) [23], the most standard GAN, results in stable training on 64×64 images. In this context, several multistage generative training methods have been proposed: Composite GAN exploits multiple generators to separately generate different parts of an image [24]; the PGGANs method adopts multiple training procedures from low resolution to high to incrementally generate a realistic image [18].

Recently, researchers applied GANs to medical imaging, mainly for image-to-image translation, such as segmentation [25], super-resolution [26], and cross-modality translation [27]. Since GANs allow for adding conditional dependency on the input information (e.g., category, image, and text), they used such conditional GANs to produce the desired corresponding images. However, GAN-based research on generating large-scale synthetic training images is limited, while the biggest challenge in this field is handling small datasets.

Differently from a very recent DA work for 64×64 CT liver lesion region of interest (ROI) classification [12], to the best of our knowledge, this is the first GAN-based whole MR image augmentation approach. This work also firstly uses PGGANs to generate 256×256 medical images. Along with classical transformations of real images, a completely different approach—generating novel realistic images using PGGANs—may become a clinical breakthrough.

27.3 Materials and Methods

27.3.1 BRATS 2016 Training Dataset

This paper exploits a dataset of 240×240 T1c brain axial MR images containing 220 high-grade glioma cases to train PGGANs with sufficient data and image resolution. These MR images are extracted from the Multimodal Brain Tumor Image Segmentation Benchmark (BRATS) 2016 [28].

27.3.2 PGGAN-Based Image Generation

27.3.2.1 Data Preparation

We select the slices from #30 to #130 among the whole 155 slices to omit initial/final slices, since they convey a negligible amount of useful information and negatively

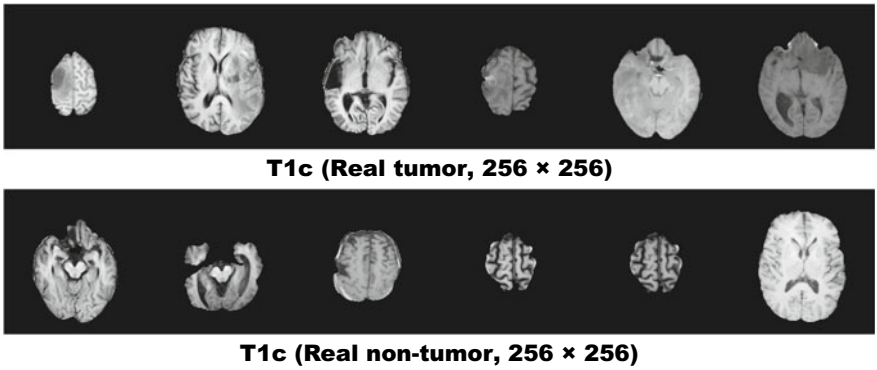

Fig. 27.2 Example of real 256 × 256 MR images used for PGGAN training

affect the training of both PGGANs and ResNet-50. For tumor detection, our whole dataset (220 patients) is divided into: (*i*) a training set (154 patients); (*ii*) a validation set (44 patients); and (*iii*) a test set (22 patients). Only the training set is used for the PGGAN training to be fair. Since tumor/non-tumor annotations are based on 3D volumes, these labels are often incorrect/ambiguous on 2D slices; so, we discard (*i*) tumor images tagged as non-tumor, (*ii*) non-tumor images tagged as tumor, (*iii*) unclear boundary images, and (*iv*) too small/big images; after all, our datasets consist of:

– Training set (5,036 tumor/3, 853 non-tumor images);
– Validation set (793 tumor/640 non-tumor images);
– Test set (1,575 tumor/1, 082 non-tumor images).

The images from the training set are zero-padded to reach a power of 2, 256 × 256 from 240 × 240 pixels for better PGGAN training. Figure 27.2 shows examples of real MR images.

27.3.2.2 PGGANs

PGGAN is a novel training method for GANs with a progressively growing generator and discriminator [18]: Starting from low resolution, newly added layers model fine-grained details as training progresses. As Fig. 27.3 shows, we adopt PGGANs to generate highly realistic and original-sized 256 × 256 brain MR images; tumor/non-tumor images are separately trained and generated.

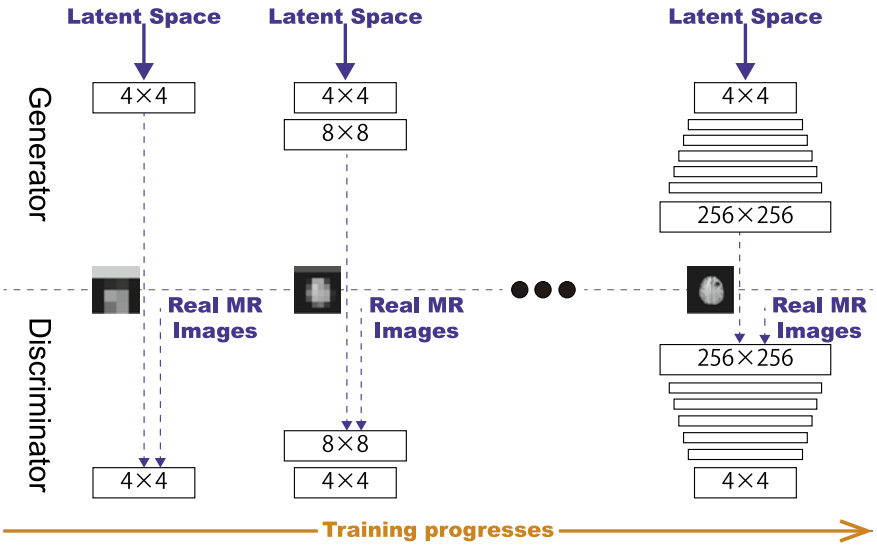

Fig. 27.3 PGGANs architecture for synthetic 256 × 256 MR image generation

27.3.2.3 PGGAN Implementation Details

We use the PGGAN architecture with the Wasserstein loss using gradient penalty [22]. Training lasts for 100 epochs with a batch size of 16 and 1.0×10^{-3} learning rate for Adam optimizer.

27.3.3 Tumor Detection Using ResNet-50

27.3.3.1 Preprocessing

To fit ResNet-50's input size, we center-crop the whole images from 240 × 240 to 224 × 224 pixels.

27.3.3.2 ResNet-50

ResNet-50 is a residual learning-based CNN with 50 layers [17]: Unlike conventional learning unreferenced functions, it reformulates the layers as learning residual functions for sustainable and easy training. We adopt ResNet-50 to detect tumors in brain MR images, i.e., the binary classification of images with/without tumors.

To confirm the effect of PGGAN-based DA, the following classification results are compared: (*i*) without DA, (*ii*) with 200,000 classical DA (100, 000 for each

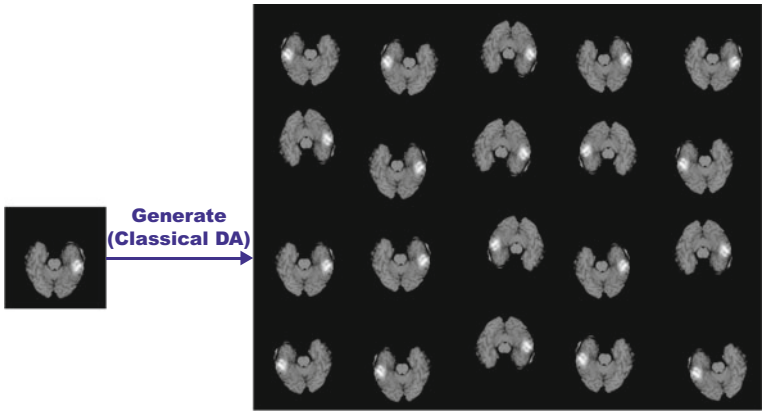

Fig. 27.4 Example of real MR image and its geometrically transformed synthetic images

class), (*iii*) with 200,000 PGGAN-based DA, and (*iv*) with both 200,000 classical DA and 200,000 PGGAN-based DA; the classical DA adopts a random combination of horizontal/vertical flipping, rotation up to 10 degrees, width/height shift up to 8%, shearing up to 8%, zooming up to 8%, and constant filling of points outside the input boundaries (Fig. 27.4). For better DA, highly unrealistic PGGAN-generated images are manually discarded.

27.3.3.3 ResNet-50 Implementation Details

We use the ResNet-50 architecture pre-trained on ImageNet with a dropout of 0.5 before the final softmax layer, along with a batch size of 192, 1.0×10^{-3} learning rate for Adam optimizer, and early stopping of 10 epochs.

27.3.4 Clinical Validation Using the Visual Turing Test

To quantitatively evaluate (*i*) how realistic the PGGAN-based synthetic images are and (*ii*) how obvious the synthetic images' tumor/non-tumor features are, we supply, in a random order, to an expert physician a random selection of:

- 50 real tumor images;
- 50 real non-tumor images;
- 50 synthetic tumor images;
- 50 synthetic non-tumor images.

Then, the physician is asked to constantly classify them as both (*i*) real/synthetic and (*ii*) tumor/non-tumor, without previous training stages revealing which is

real/synthetic and tumor/non-tumor; here, we only show successful cases of synthetic images, as we can discard failed cases for better data augmentation. The so-called visual Turing test [19] is used to probe the human ability to identify attributes and relationships in images, also in evaluating the visual quality of GAN-generated images [9]. Similarly, this applies to medical images in clinical environments [11, 12], wherein physicians' expertise is critical.

27.3.5 Visualization Using t-SNE

To visually analyze the distribution of both (*i*) real/synthetic and (*ii*) tumor/non-tumor images, we use t-distributed stochastic neighbor embedding (t-SNE) [29] on a random selection of:

- 300 real non-tumor images;
- 300 geometrically transformed non-tumor images;
- 300 PGGAN-generated non-tumor images;
- 300 real tumor images;
- 300 geometrically transformed tumor images;
- 300 PGGAN-generated tumor images.

Only 300 images per each category are selected for better visualization. t-SNE is a machine learning algorithm for dimensionality reduction to represent high-dimensional data into a lower-dimensional (2D/3D) space. It nonlinearly adapts to input data using perplexity, which balances between the data's local and global aspects.

27.3.5.1 t-SNE Implementation Details

We use t-SNE with a perplexity of 100 for 1,000 iterations to obtain a 2D visual representation.

27.4 Results

This section shows how PGGANs generate synthetic brain MR images. The results include instances of synthetic images, their quantitative evaluation by an expert physician, and their influence on tumor detection.

27.4.1 MR Images Generated by PGGANs

Figure 27.5 illustrates examples of synthetic tumor/non-tumor images by PGGANs. In our visual confirmation, for about 75% of cases, PGGANs successfully capture

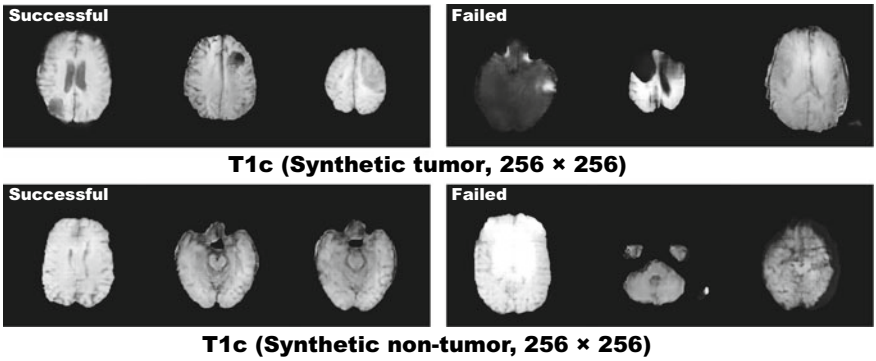

Fig. 27.5 Example of synthetic MR images yielded by PGGANs: **a** successful cases and **b** failed cases

the T1c-specific texture and tumor appearance while maintaining the realism of the original brain MR images; however, for about 25% of cases, the generated images lack clear tumor/non-tumor features or contain unrealistic features, such as hyper-intensity, gray contours, and odd artifacts.

27.4.2 Tumor Detection Results

Table 27.1 shows the classification results for detecting brain tumors with/without DA techniques. As expected, the test accuracy improves by 0.64% with the additional 200, 000 geometrically transformed images for training. When only the PGGAN-based DA is applied, the test accuracy decreases drastically with almost 100% of sensitivity and 6.84% of specificity, because the classifier recognizes the synthetic images' prevailed unrealistic features as tumors, similarly to anomaly detection.

Table 27.1 Binary classification results for detecting brain tumors with/without DA

Experimental condition	Accuracy (%)	Sensitivity (%)	Specificity (%)
ResNet-50 (w/o DA)	90.06	85.27	97.04
ResNet-50 (w/200k classical DA)	90.70	88.70	93.62
ResNet-50 (w/200k PGGAN-based DA)	62.02	**99.94**	6.84
ResNet-50 (w/200k classical DA + 200k PGGAN-based DA)	**91.08**	86.60	**97.60**

Table 27.2 Visual Turing test results by a physician for classifying real (*R*) versus synthetic (*S*) images and tumor (*T*) vs non-tumor (*N*) images

Real/synthetic classification	*R* as *R*	*R* as *S*	*S* as *R*	*S* as *S*
78.5%	58	42	1	99
Tumor/non-tumor classification	*T* as *T*	*T* as *N*	*N* as *T*	*N* as *N*
90.5%	82	18 (*R*: 5, *S*: 13)	1 (*S*: 1)	99

However, surprisingly, when it is combined with the classical DA, the accuracy increases by 1.02% with higher sensitivity and specificity; this could occur because the PGGAN-based DA fills the real image distribution uncovered by the original dataset, while the classical DA provides the robustness on training for most cases.

27.4.3 Visual Turing Test Results

Table 27.2 shows the confusion matrix for the visual Turing test. Differently from our previous work on GAN-based 64 × 64/128 × 128 MR image generation, the expert physician easily recognizes 256 × 256 synthetic images [13], while tending also to classify real images as synthetic; this can be attributed to high resolution associated with more difficult training and detailed appearance, making artifacts stand out, which is coherent to the ResNet-50's low tumor detection accuracy with only the PGGAN-based DA. Generally, the physician's tumor/non-tumor classification accuracy is high and the synthetic images successfully capture tumor/non-tumor features. However, unlike non-tumor images, the expert recognizes a considerable number of tumor images as non-tumor, especially on the synthetic images; this results from the remaining real images' ambiguous annotation, which is amplified in the synthetic images trained on them.

27.4.4 t-SNE Result

As presented in Fig. 27.6, tumor/non-tumor images' distribution shows a tendency that non-tumor images locate from top left to bottom right and tumor images locate from top right to center, while the distinction is unclear with partial overlaps. Classical DA covers a wide range, including zones without any real/GAN-generated images, but tumor/non-tumor images often overlap there. Meanwhile, PGGAN-generated images concentrate differently from real images, while showing more frequent overlaps than the real ones; this probably derives from those synthetic images with unsatisfactory realism and tumor/non-tumor features.

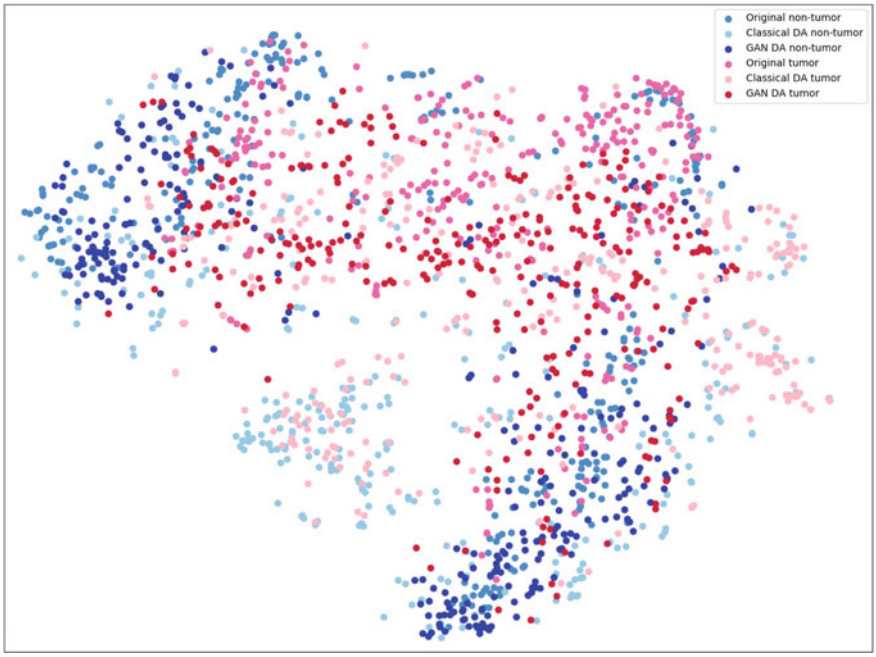

Fig. 27.6 t-SNE result on six categories, with 300 images per each category: **a** real tumor/non-tumor images; **b** geometrically transformed tumor/non-tumor images; and **c** PGGAN-generated tumor/non-tumor images

27.5 Conclusion

Our preliminary results show that PGGANs can generate original-sized 256×256 realistic brain MR images and achieve higher performance in tumor detection, when combined with classical DA. This occurs because PGGANs' multistage image generation obtains good generalization and synthesizes images with the real image distribution unfilled by the original dataset. However, considering the visual Turing test and t-SNE results, yet unsatisfactory realism with high resolution strongly limits DA performance, so we plan to (*i*) generate only realistic images and then (*ii*) refine synthetic images more similar to the real image distribution.

For (*i*), we can map an input random vector onto each training image [30] and generate images with suitable vectors, to control the divergence of generated images; virtual adversarial training could be also integrated to control the output distribution. Moreover, (*ii*) can be achieved by GAN/VAE-based image-to-image translation, such as unsupervised image-to-image translation networks [31], considering SimGAN's remarkable performance improvement after refinement [9]. Moreover, we should further avoid real images with ambiguous/inaccurate annotation for better tumor detection.

Overall, our novel PGGAN-based DA approach sheds light on diagnostic and prognostic medical applications, not limited to tumor detection; future studies are needed to extend our encouraging results.

Acknowledgements This work was partially supported by the Graduate Program for Social ICT Global Creative Leaders of the University of Tokyo by JSPS.

References

1. Rundo, L., Militello, C., Russo, G., Vitabile, S., Gilardi, M.C., Mauri, G.: GTVcut for neuro-radiosurgery treatment planning: an MRI brain cancer seeded image segmentation method based on a cellular automata model. Nat. Comput. **17**(3), 521–536 (2018)
2. Rundo, L., Militello, C., Vitabile, S., Russo, G., Pisciotta, P., Marletta, F., Ippolito, M., DArrigo, C., Midiri, M., Gilardi, M.C.: Semi-automatic brain lesion segmentation in Gamma Knife treatments using an unsupervised fuzzy c-means clustering technique. In: Advances in Neural Networks: Computational Intelligence for ICT. Volume 54 of Smart Innovation, Systems and Technologies, pp. 15–26. Springer (2016)
3. Bevilacqua, V., Brunetti, A., Cascarano, G.D., Palmieri, F., Guerriero, A., Moschetta, M.: A deep learning approach for the automatic detection and segmentation in autosomal dominant polycystic kidney disease based on Magnetic Resonance images. In: Proceedings of International Conference on Intelligent Computing (ICIP), pp. 643–649. Springer (2018)
4. Brunetti, A., Carnimeo, L., Trotta, G.F., Bevilacqua, V.: Computer-assisted frameworks for classification of liver, breast and blood neoplasias via neural networks: a survey based on medical images. Neurocomputing **335**, 274–298 (2018)
5. Havaei, M., Davy, A., Warde-Farley, D., Biard, A., Courville, A., Bengio, Y., et al.: Brain tumor segmentation with deep neural networks. Med. Image Anal. **35**, 18–31 (2017)
6. Kamnitsas, K., Ledig, C., Newcombe, V.F.J., Simpson, J.P., Kane, A.D., Menon, D.K., et al.: Efficient multi-scale 3D CNN with fully connected CRF for accurate brain lesion segmentation. Med. Image Anal. **36**, 61–78 (2017)
7. Ronneberger, O., Fischer, P., Brox, T.: U-Net: convolutional networks for biomedical image segmentation. In: Proceedings of International Conference on Medical Image Computing and Computer-Assisted Intervention (MICCAI), pp. 234–241 (2015)
8. Milletari, F., Navab, N., Ahmadi, S.: V-Net: Fully convolutional neural networks for volumetric medical image segmentation. In: Proceedings of International Conference on 3D Vision (3DV), pp. 565–571. IEEE (2016)
9. Shrivastava, A., Pfister, T., Tuzel, O., Susskind, J., Wang, W., Webb, R.: Learning from simulated and unsupervised images through adversarial training. In: Proceedings of Conference on Computer Vision and Pattern Recognition (CVPR), pp. 2107–2116. IEEE (2017)
10. Costa, P., Galdran, A., Meyer, M.I., Niemeijer, M., Abràmoff, M., Mendona, A.M., Campilho, A.: End-to-end adversarial retinal image synthesis. IEEE Trans. Med. Imaging **37**(3), 781–791 (2018)
11. Chuquicusma, M.J.M., Hussein, S., Burt, J., Bagci, U.: How to fool radiologists with generative adversarial networks? a visual Turing test for lung cancer diagnosis. In: Proceedings of International Symposium on Biomedical Imaging (ISBI), pp. 240–244. IEEE (2018)
12. Frid-Adar, M., Diamant, I., Klang, E., Amitai, M., Goldberger, J., Greenspan, H.: GAN-based synthetic medical image augmentation for increased CNN performance in liver lesion classification. Neurocomputing **321**, 321–331 (2018)
13. Han, C., Hayashi, H., Rundo, L., Araki, R., Shimoda, W., Muramatsu, S., et al.: GAN-based synthetic brain MR image generation. In: Proceedings of International Symposium on Biomedical Imaging (ISBI), pp. 734–738. IEEE (2018)

14. Militello, C., Rundo, L., Vitabile, S., et al.: Gamma knife treatment planning: MR brain tumor segmentation and volume measurement based on unsupervised fuzzy c-means clustering. Int. J. Imaging Syst. Technol. **25**(3), 213–225 (2015)
15. Rundo, L., Stefano, A., Militello, C., Russo, G., Sabini, M.G., D'Arrigo, C., Marletta, F., Ippolito, M., Mauri, G., Vitabile, S., Gilardi, M.C.: A fully automatic approach for multimodal PET and MR image segmentation in Gamma Knife treatment planning. Comput. Methods Programs Biomed. **144**, 77–96 (2017)
16. Szegedy, C., Ioffe, S., Vanhoucke, V., Alemi, A.A.: Inception-v4, inception-resnet and the impact of residual connections on learning. In: Proceedings of AAAI Conference on Artificial Intelligence (AAAI) (2017)
17. He, K., Zhang, X., Ren, S., Sun, J.: Deep residual learning for image recognition. In: Proceedings of Conference on Computer Vision and Pattern Recognition (CVPR), pp. 770–778. IEEE (2016)
18. Karras, T., Aila, T., Laine, S., Lehtinen, J.: Progressive growing of GANs for improved quality, stability, and variation. In: Proceedings of International Conference on Learning Representations (ICLR). arXiv preprint arXiv:1710.10196v3 (2018)
19. Salimans, T., Goodfellow, I., Zaremba, W., Cheung, V., Radford, A., Chen, X.: Improved techniques for training GANs. In: Advances in Neural Information Processing Systems (NIPS), pp. 2234–2242 (2016)
20. Goodfellow, I., Pouget-Abadie, J., Mirza, M., Xu, B., Warde-Farley, D., Ozair, S., et al.: Generative adversarial nets. In: Advances in Neural Information Processing Systems (NIPS), pp. 2672–2680 (2014)
21. Zhu, J.Y., Park, T., Isola, P., Efros, A.A.: Unpaired image-to-image translation using cycle-consistent adversarial networks. In: Proceedings of International Conference on Computer Vision (ICCV), pp. 2242–2251. IEEE (2017)
22. Gulrajani, I., Ahmed, F., Arjovsky, M., Dumoulin, V., Courville, A.C.: Improved training of Wasserstein GANs. In: Advances in Neural Information Processing Systems, pp. 5769–5779 (2017)
23. Radford, A., Metz, L., Chintala, S.: Unsupervised representation learning with deep convolutional generative adversarial networks. In: Proceedings of International Conference on Learning Representations (ICLR). arXiv preprint arXiv:1511.06434 (2016)
24. Kwak, H., Zhang, B.: Generating images part by part with composite generative adversarial networks. arXiv preprint arXiv:1607.05387 (2016)
25. Xue, Y., Xu, T., Zhang, H., Long, L.R., Huang, X.: SegAN: Adversarial network with multi-scale L_1 loss for medical image segmentation. Neuroinformatics **16**(3–4), 383–392 (2018)
26. Mahapatra, D., Bozorgtabar, B., Hewavitharanage, S., Garnavi, R.: Image super resolution using generative adversarial networks and local saliency maps for retinal image analysis. In: Proceedings of International Conference on Medical Image Computing and Computer-Assisted Intervention (MICCAI), pp. 382–390 (2017)
27. Nie, D., Trullo, R., Lian, J., Petitjean, C., Ruan, S., Wang, Q., Shen, D.: Medical image synthesis with context-aware generative adversarial networks. In: Proceedings of International Conference on Medical Image Computing and Computer-Assisted Intervention (MICCAI), pp. 417–425 (2017)
28. Menze, B.H., Jakab, A., Bauer, S., et al.: The multimodal brain tumor image segmentation benchmark (BRATS). IEEE Trans. Med. Imaging **34**(10), 1993–2024 (2015)
29. van der Maaten, L., Hinton, G.: Visualizing data using t-SNE. J. Mach. Learn. Res. **9**, 2579–2605 (2008)
30. Schlegl, T., Seeböck, P., Waldstein, S.M., Schmidt-Erfurth, U., Langs, G.: Unsupervised anomaly detection with generative adversarial networks to guide marker discovery. In: Proceedings of International Conference on Information Processing in Medical Imaging (IPMI), pp. 146–157 (2017)
31. Liu, M.Y., Breuel, T., Kautz, J.: Unsupervised image-to-image translation networks. In: Advances in Neural Information Processing Systems (NIPS), pp. 700–708 (2017)